Supplemental Figures and Legends

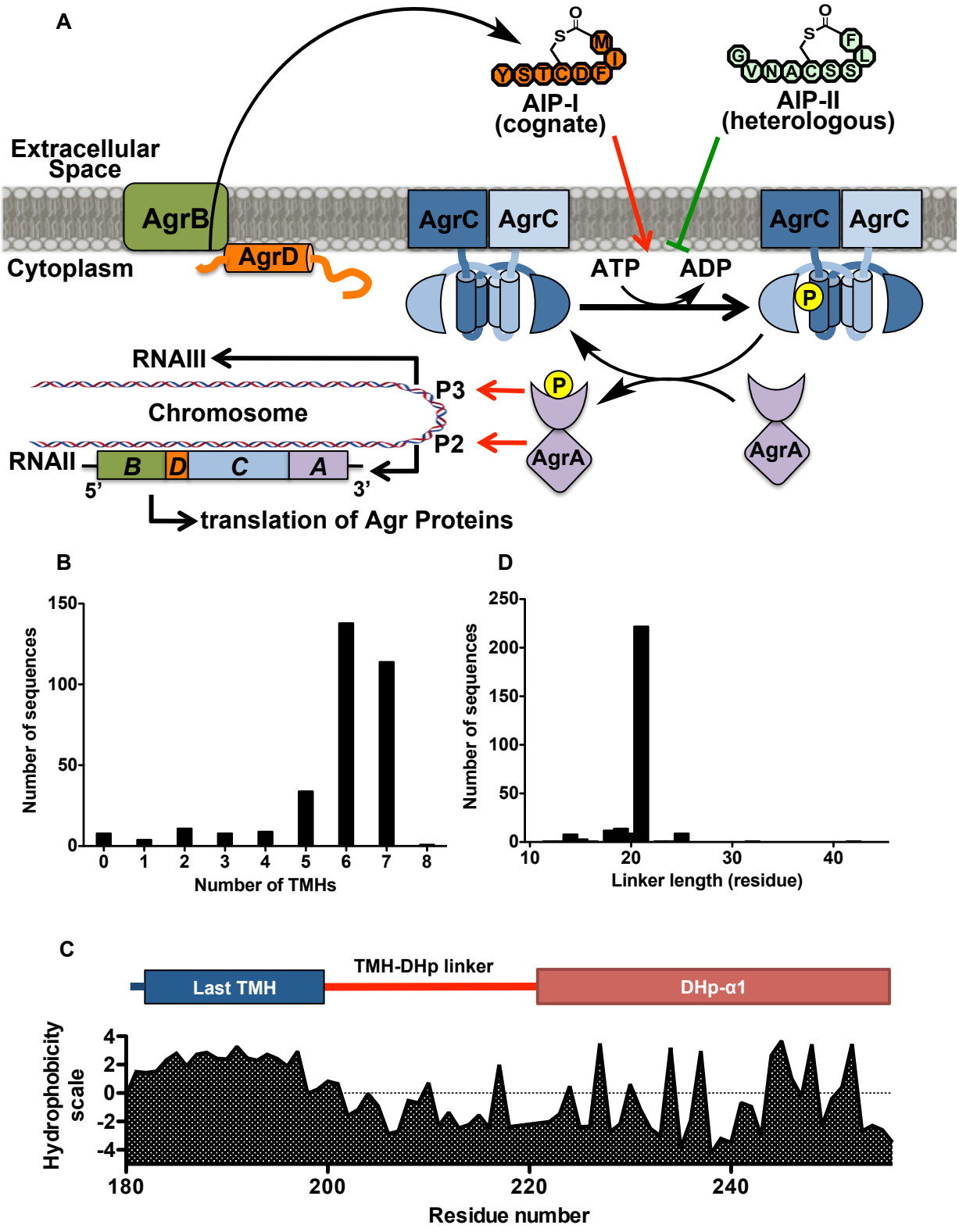

Figure S1. The *agr* quorum sensing circuit in *S. aureus* and analysis of the HPK10 subfamily, related to Figure 1.

(A) The diagram depicts a group I *agr* circuit. Group-I AgrD precursor peptide (orange) is processed into mature AIP-I. Production and secretion of AIP-I requires an integral membrane protein, AgrB (green). AIP-I binds to the receptor histidine kinase, AgrC-I, and induces its autokinase activity. Activated AgrC-I relays the phosphoryl group to the RR, AgrA, which then activates transcription of both P2 and P3 operons in the *agr* locus. This results in a positive feedback on the circuit and an up-regulation of the P3 transcript, RNAIII, which controls the expression of *agr*-related virulence genes. A heterologous AIP, AIP-II, suppresses RNAIII production through binding to AgrC-I and inhibiting its autokinase activity. **(B)** Predicted number of TMHs in the 326 members of the HPK10 subfamily using the software package, TMHMM-2.0. (**C**) Convergence of the last TMH and DHp-α1 in the multiple sequence alignment of 286 HPK10 sequences predicted to have five or more TMHs. Plot shows the averaged hydrophobicity scale at each position aligned to AgrC-I$^{180\text{-}256}$. Predicted domains of AgrC-I are shown above with color coding as in Figure 1A. **(D)** Predicted length of the TMH-DHp linker (in residues) in the multiple sequence alignment of the 285 sequences.

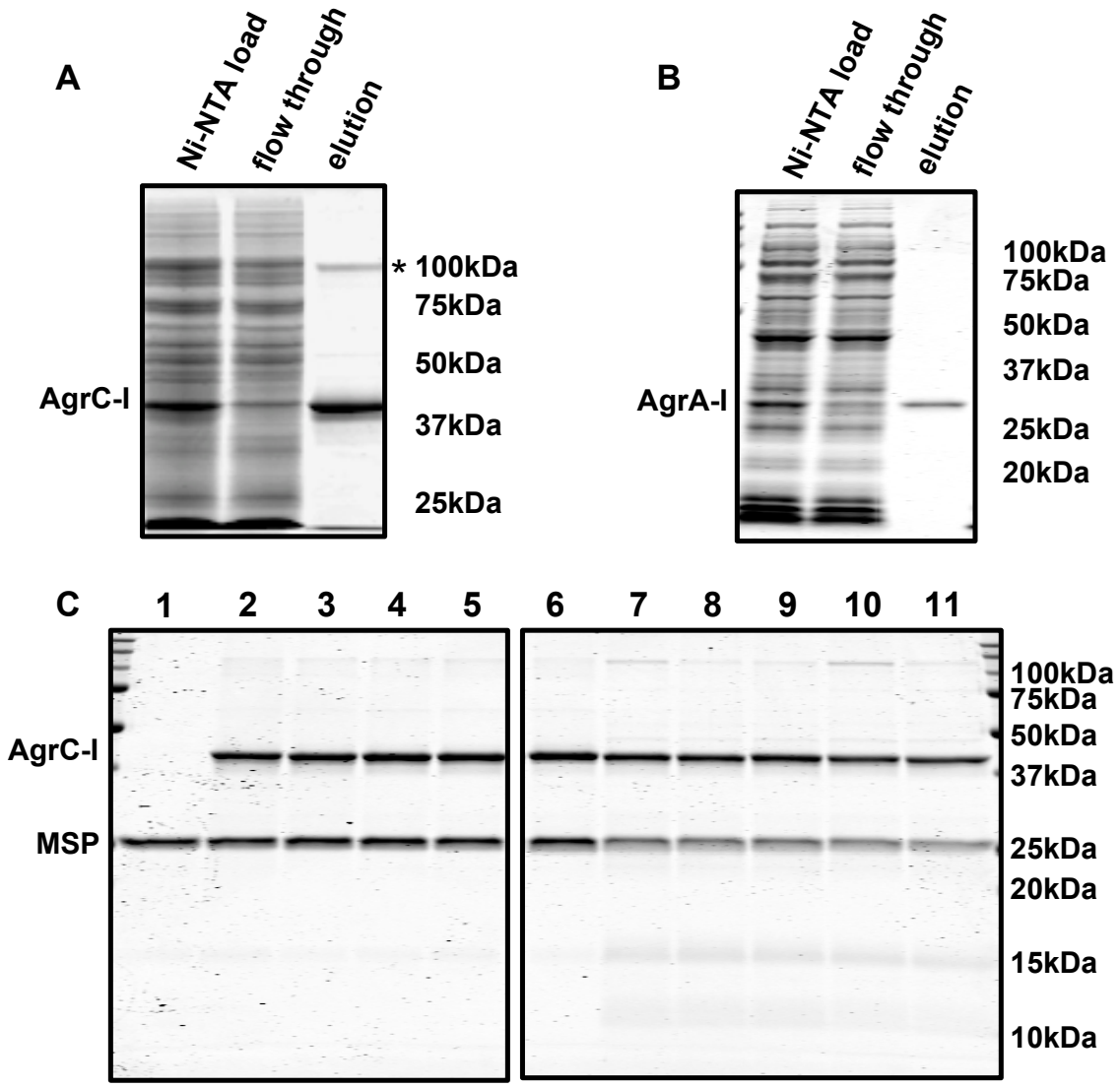

Figure S2. SDS-PAGE analysis of proteins and nanodiscs, related to Figure 2

(A and **B)** Purification of **(A)** AgrC-I from *E. coli* membrane extract and **(B)** AgrA-I from *E. coli* total soluble lysate as analyzed by SDS-PAGE with CBB-stain. Bands corresponding to the target proteins are indicated. Asterisk indicates a 100-kDa protein co-purified with AgrC-I, which would be removed in subsequent chromatographic steps (see panel C, lane 2). **(C)** SDS-PAGE analysis of purified nanodiscs. Lane 1, empty discs; lanes 2-11 (left to right), nanodiscs incorporated with wild-type, R238H, H239Q, G394A/G396A, S109V/S116I, L205C, K206C, E207C, M208C and K209C variants of AgrC-I. Bands corresponding to AgrC-I and MSP are indicated.

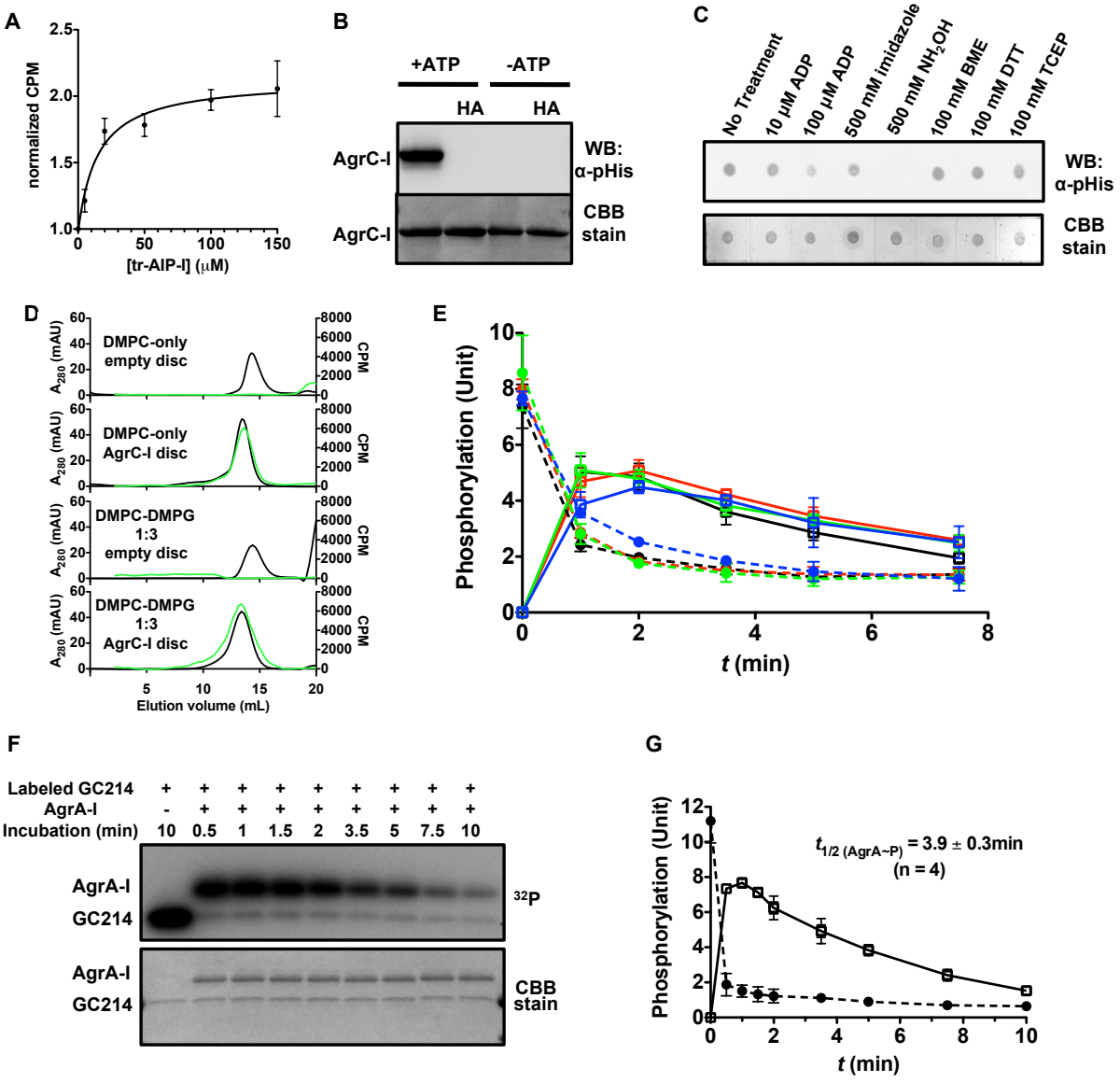

Figure S3. Biochemical activities associated with reconstituted AgrC-I, related to Figure 3.

(A) Saturation of tr-AIP-I binding to AgrC-I. AgrC-I discs were treated with tr-AIP-I at indicated concentrations and then incubated with 20 μM [γ-^{32}P] ATP at 37 ^{o}C for 40 minutes. Plot shows pHis levels normalized to the peptide-free reaction versus tr-AIP-I concentration, fit to a saturation-binding model. Error bars = S.D. (n = 3). **(B)** Hydroxylamine (HA) treatment of phosphorylated AgrC-I. AgrC-I discs were phosphorylated with ATP (lanes 1 and 2) as described in Figure 3A or mock-treated (lanes 3 and 4) and then incubated with either buffer (lanes 1 and 3) or 500 mM HA (lanes 2 and 4) at 37^{o}C for 5 min. pHis levels of AgrC-I were then analyzed by western blotting as in Figure 3A. **(C)** Stability test of phosphorylation on AgrC-

I. Pre-phosphorylated AgrC-I discs (refer to Figure S4G) were treated with indicated reagent at 37^{o}C for 20 min in a buffer containing 50 mM Tris, pH = 8.0, 100 mM NaCl, 5mM $MgCl_2$. pHis levels of AgrC-I were analyzed by anti-pHis immunobloting (upper). The blot was CBB-stained thereafter as a loading control (lower). **(D)** Co-migration assay of a FAM-AIP-I (refer to Figure S4B) with selected nanodisc samples: AgrC-I or empty discs assembled with DMPC only or a DMPC-DMPG mixture were incubated with excess FAM-AIP-I and analyzed by SEC. UV and fluorescence detection of the chromatograms are overlaid. **(E)** Quantification of the autoradiogram in Figure 3H showing phosphorylation levels of GC214 (close circles, dotted connecting lines) and AgrA-I (Open squares, solid connecting lines) as a function of time. Data from the reaction without AgrC-I discs (black), with AgrC-I discs alone (red), AgrC-I discs plus AIP-I (green) and AgrC-I discs plus AIP-II (blue) were plotted as mean ± S.D. (n = 3). **(F and G)** Kinetics of the self-catalyzed dephosphorylation of AgrA-I. AgrA-I was treated with pre-labeled GC214 as described for Figure 3H. One representative autoradiogram **(F)** and the quantification result **(G)** of the time course are shown. In **(G)**, phosphorylation levels of GC214 and AgrA-I were plotted as mean ± S.D. (n = 4); data symbols and connecting lines are same as in **(E)**. AgrA-I phosphorylation levels after 1 min were fit to a first-order decay model.

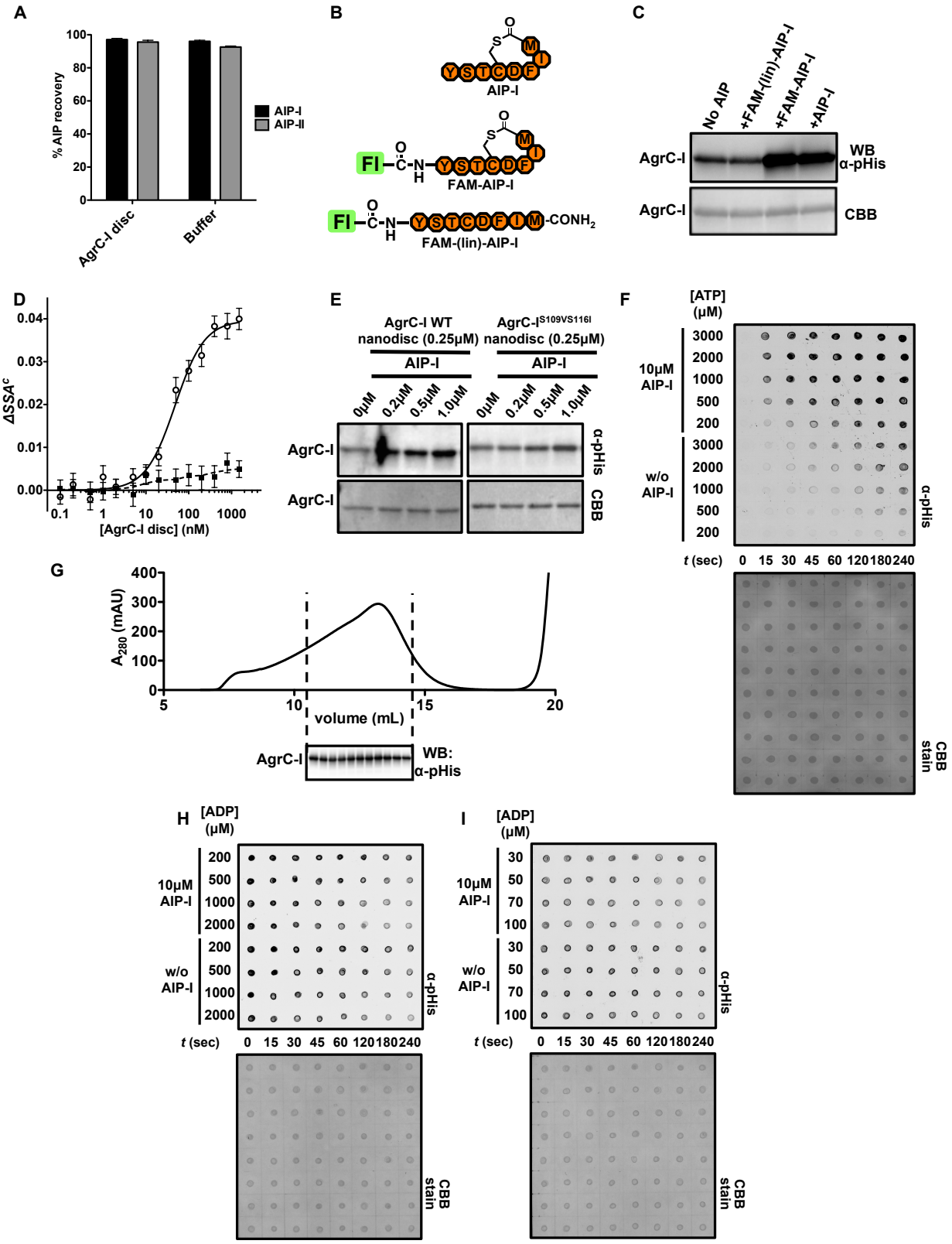
A
% AIP recovery
AIP-I
AIP-II
AgrC-I disc
Buffer
B
AIP-I
FAM-AIP-I
FAM-(lin)-AIP-I
C
No AIP
+FAM-(lin)-AIP-I
+FAM-AIP-I
+AIP-I
AgrC-I
WB α-pHis
CBB
D
ΔSSA^c
[AgrC-I disc] (nM)
E
AgrC-I WT nodisc (0.25μM)
AgrC-I^S109VS116I nodisc (0.25μM)
AIP-I
0μM
0.2μM
0.5μM
1.0μM
α-pHis
CBB
F
[ATP] (μM)
10μM AIP-I
w/o AIP-I
t (sec)
CBB stain
G
A280 (mAU)
volume (mL)
WB: α-pHis
H
[ADP] (μM)
I

Figure S4. Supplemental data related to ligand-binding and kinetic studies of AgrC-I, related to Figure 4.

(A) Stability test of AIPs in the presence of AgrC-I discs: AIP-I or AIP-II (2 nmol) were incubated in the presence or absence of AgrC-I discs (0.2 nmol) at 37°C. Percentage of intact AIP that remained after each treatment was quantified using HPLC (See Extended Experimental Procedures) and plotted as mean ± SD (n = 3). (**B**) Schematic presentation of AIP-I, FAM-AIP-I and FAM-(lin)-AIP-I. **(C)** AgrC-I discs were phosphorylated as described in Figure 3A with the indicated peptides (10 μM) for 3 minutes. The reactions were then analyzed by western blotting as in Figure 3A. **(D)** Titration of FAM-AIP-I with AgrC-I^{S109VS116I} dimers. As in described Figure 4B, ΔSSA^c was plotted as a function of AgrC-I^{S109VS116I} discs added (closed circle) and connected with a smoothed curve (dashed curve). Result from one representative titration is shown. Data points and fitted curve for the titration with wild-type AgrC-I discs as in Figure 4B are shown for comparison (open square and solid curve). **(E)** Autokinase activation of AgrC-I^{S109VS116I} dimers: 0.25 μM nanodiscs containing wild-type AgrC-I dimers (left four lanes) or AgrC-I^{S109VS116I} mutant dimers (right four lanes) were incubated with 1 mM ATP, 5 mM $MgCl_2$ and AIP-I at indicated concentrations at 37°C for 3min. The reactions were then analyzed as in Figure 3A. **(F)** Time-courses of autokinase reactions: AgrC-I discs were incubated at 37°C with ATP (at indicated concentration) and 5 mM $MgCl_2$ in the presence or absence of 10 μM AIP-I peptide. Aliquots were removed from each reaction at indicated time points and spotted in a row on the blotting membrane. pHis levels of AgrC-I were analyzed by anti-pHis immunobloting. The membrane was CBB-stained thereafter for loading control. **(G)** Pre-phosphorylated AgrC-I discs analyzed by SEC. Fractions collected between the dashed lines were further analyzed by western blotting with anti-pHis antibody. **(H** and **I)** Time-courses of reverse autokinase reactions: pre-phosphorylated AgrC-I discs were incubated at 37°C with ADP at indicated concentration and 5 mM $MgCl_2$ in the presence or absence of 10 μM AIP-I peptide. Reactions were analyzed as in panel G.

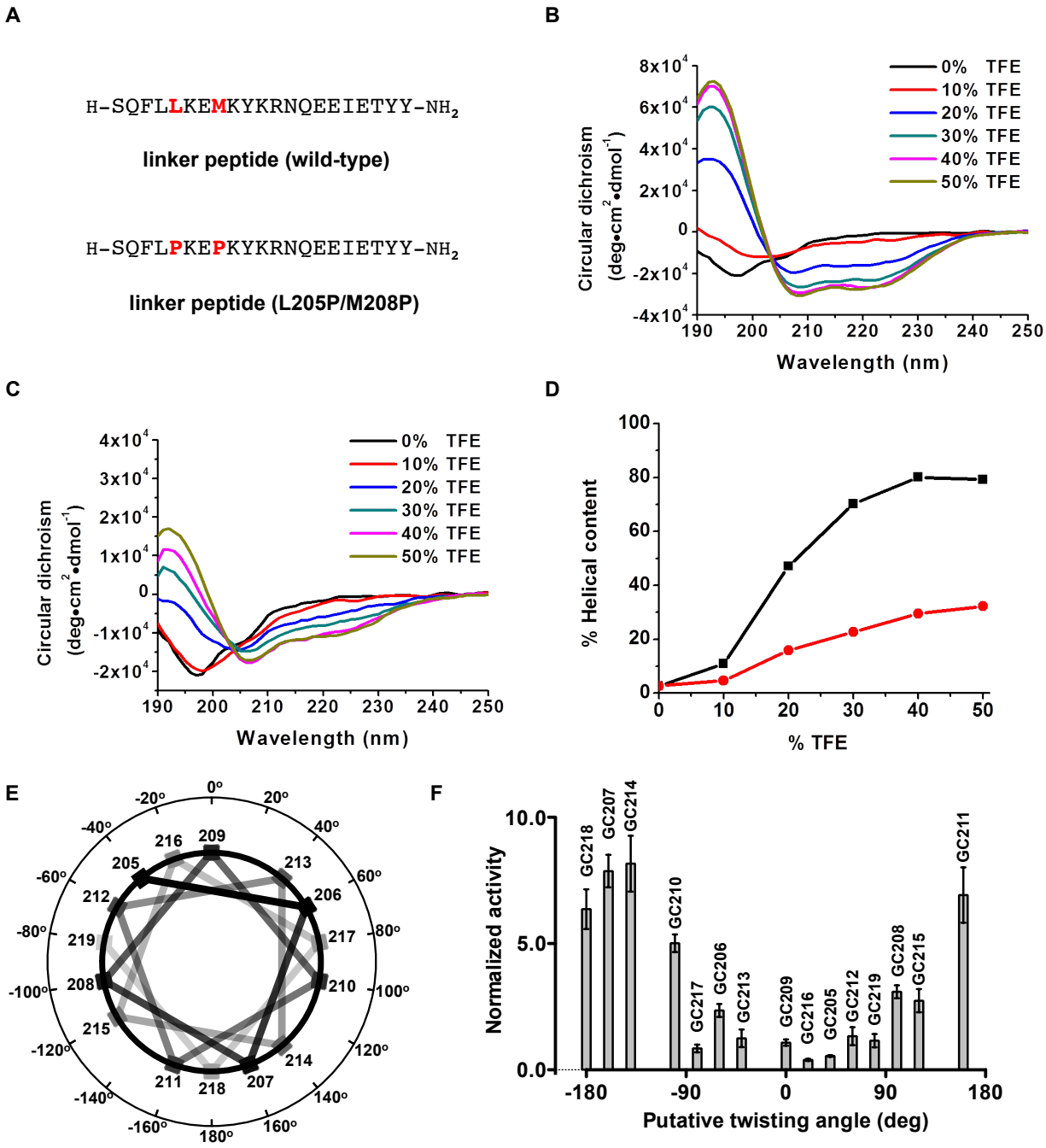

Figure S5. Circular dichroism (CD) spectroscopy analysis of TMH-DHp linker peptides and the rheostat-like behavior of AgrC-I^{HK}, related to Figure 5.

(A) Sequence of the wild-type linker peptide (upper) and the L205PM208P mutant peptide (lower). Mutated residues are highlighted in red. **(B and C)** CD spectroscopy. Each peptide was dissolved at 15 μM in buffer solutions (10 mM phosphate, pH = 7.0 and 50 mM NaF) containing the indicated percentage of TFE (v/v). The CD spectrum of each solution was recorded at 20 ^{o}C

and corrected for solvent background. Spectra for the wildtype (**B**) and mutant peptide **(C)** are shown. **(D)** Helical content of linker peptides: plot shows calculated helical content as a function of % TFE for the wild-type (black) and L205P/M208P mutant (red) peptides. **(E)** Classical helical wheel showing the angle (θ) by which each position on the linker helix deviates from position 209. Since the linker conformation in GC209 resembles that of AgrC-I in the resting state (refer to Figure S6C), the putative twisting angle imposed to the linker helices in each GCN4-AgrC-I chimera should be the inverse number of θ for its junction residue position. (**F**) Plot shows activity of all 15 GCN4-AgrC-I chimeras versus the putative twisting angle. Error bar = S.D. (n = 3).

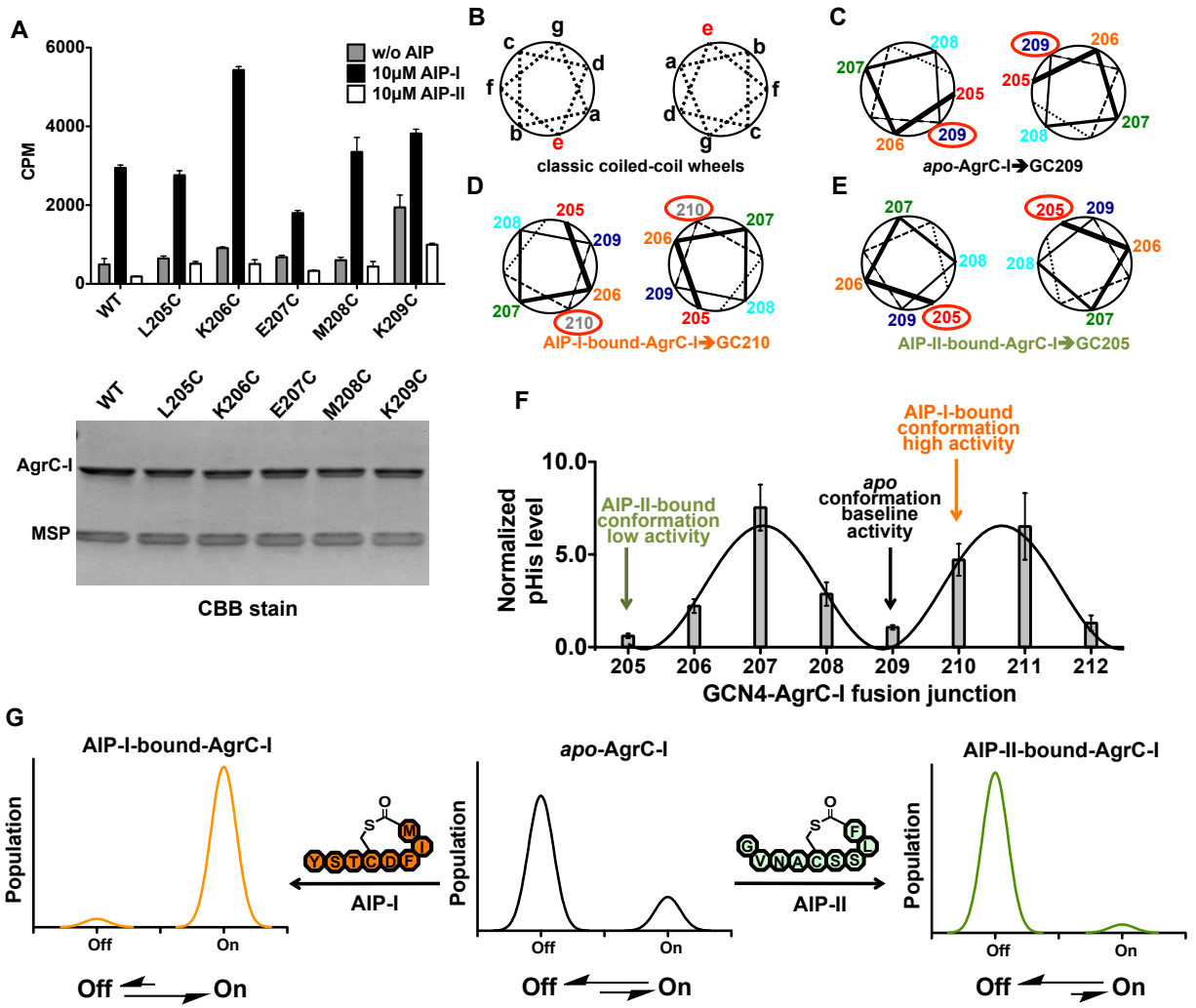

Figure S6. Role of the TMH-DHp linker conformation AgrC-I signaling, related to Figure 6. **(A)** Autokinase activities of AgrC-I cysteine single-point mutants. Nanodiscs containing wild-type or cysteine-mutant AgrC-I dimers were incubated with 20 μM [γ-^{32}P]-ATP, 5 mM $MgCl_2$ and excess AIP peptide (as indicated) at 37°C for 40min. ^{32}P-labeled AgrC-I in each reaction was quantified through scintillation counting (upper). Error bar = SD (n = 3). Stock solutions of all six nanodiscs were analyzed by SDS-PAGE followed by CBB staining as a loading control (below). **(B)** Helical wheels for a classic coiled-coil: position 'e', the predicted register of the junction residue in the GCN4-AgrC-I chimeras, is highlighted in red. **(C** to **E)** Identification of conformational surrogates of full-length AgrC-I. Linker helical wheels for **(C)** *apo*-, **(D)** AIP-I-bound, and **(E)** AIP-II bound states are adapted from Figure 6C. Positions assigned or predicted to locate closest to position 'e' are highlighted with red ovals. GCN4-AgrC-I chimeras with GCN4$^{1\text{-}25}$ fused to these positions, i.e. GC209, GC210 and GC205 are identified as surrogates of

full-length AgrC-I under three activity states, respectively. **(F)** Autokinase activities of GCN4-AgrC-I chimera surrogates of full-length AgrC-I. Plot shows normalized phosphorylation levels of chimera proteins, GC205 through GC212, as found in Figure 5F as a function of junction residue positions (with AgrC-I numbering). Conformational surrogate of each activity state is marked with an arrow. **(G)** An alternative model in which the TMH-DHp linkers are in equilibrium between an 'on' state associated with high autokinase activity and an 'off' state with low activity. Binding of activator or inhibitor AIPs shifts the equilibrium position.

Supplemental Table Legends

Table S1 All RHK hits from database search, related to Figure 1.

[a]: The query sequence for the first round of database search;

[b]: Query sequences for the second round of database search;

[c]: Founding members of the HPK10 subfamily (Grebe and Stock, 1999). 7 sequences in the table covers 12 out of 15 founding with at >75% sequence identity. The rest 3 are not deposited in the Refseq database.

[d]: There is controversy on whether the class Mollicutes should be placed in the phylum Firmicutes or Tenericutes (Davis et al., 2013).

Extended Experimental Procedures

General Materials

All buffering salts, media for bacterial cultures, isopropyl-β-D-thiogalactopyranoside (IPTG), 1, 4-dithiothreitol (DTT), tris-(2-carboxyethyl) phosphine hydrochloride (TCEP), iodoacetamide, Coomassie brilliant blue, phenylmethylsulfonyl fluoride (PMSF) and nitrocellulous membranes were purchased from Fisher Scientific (Pittsburgh, PA). All antibiotics, non-labeled nucleotides for AgrC-I-related assays, *N, N*-dimethylformamide (DMF), dimethylsulfoxide (DMSO), 2,2,2-trifluoroethanol (TFE), *N, N*-diisopropylethylamine (DIEA), piperidine, triisopropylsilane (TIS), β-mercaptoethanol (BME), bovine serum albumin (BSA), and Eastman KODAK BioMax Film were purchased from Sigma-Aldrich (St. Louis, MO). All 9-fluorenylmethyloxycarbonyl (Fmoc) protected amino acids, Rink-amide MBHA resin and HATU were purchased from Novabiochem. [γ-^{32}P]-Adenosine triphosphate and Ultima Gold Cocktail was from PerkinElmer (Waltham, MA). All lipids were purchased from Avanti Polar lipids (Alabaster, AL) and all detergents were

obtained from Anatrace (Maumee, OH). Trifluoroacetic acid (TFA) was from Halocarbon (North Augusta, SC). Nickel-nitrilotriacetic acid (Ni-NTA) resin and KOD polymerase was from Novagen (Gibbstown, NJ). The QuikChange Site-Directed Mutagenesis kit was from Agilent (La Jolla, CA). T4 DNA ligase, restriction enzymes and the Phusion High-Fidelity PCR kit were from New England Biolabs (Ipswich, MA). DNA purification kits (QIAprep spin minikit, QIAquick gel extraction kit, QIAquick PCR purification kit) were from Qiagen (Valencia, CA). Sub-cloning efficient DH5α competent cells and One Shot BL21(DE3) chemically competent *E.coli* were purchased from Invitrogen (Carlsbad, CA) and used to generate "in-house" high-competency cell lines. Oligonucleotides were purchased from Integrated DNA Technologies (Coralville, IA). Codon-optimized cDNAs were generated synthetically and purchased from GENEWIZ (South Plainfield, NJ). All plasmids used in this study were sequenced by GENEWIZ. Centrifugal filtration units were from Sartorius (Goettingen, Germany). All denaturing gels, PVDF membrane (0.2 μm), Bio-Beads SM2 Adsorbent and goat anti-rabbit monoclonal antibody were from Bio-Rad (Hercules, CA). IRDye 800CW goat anti-rabbit IgG was from LI-COR Biotechnology (Lincoln, NE). The pan-specific antibody recognizing pHis (pHis) was purified from the anti-pHis polyclonal antiserum. Natural AIPs and their analogs were synthesized and purified as previously described (Lyon et al., 2002) and solublized into 1 mM stock solution in DMSO.

General Equipments

Solid-phase peptide synthesis (SPPS) was carried on a Liberty Synthesizer (CEM, Matthews, NC). Size exclusion chromatography was carried out on an ÄKTA FPLC system from GE Healthcare using a Superdex200 10/300 column or a Superose6 10/30 HR column. For all runs, proteins were eluted over 1.35 column volumes of buffer (flow rate: 0.4 mL/min). For SEC-MALS experiments, the ÄKTA FPLC system was connected in tandem to a DAWN HELEOS-II multi-angle light scattering instrument and OptiLab TrEX differential refractometer. Ion-exchange chromatography was performed on the same FPLC instrument system using a Hiprep Q FF 16/10 column. Analytical RP-HPLC was performed on Hewlett-Packard 1100 and 1200 series instruments equipped with a C_{18} Vydac column (5μm, 4.6 x 150 mm) at a flow rate of 1 mL/min. All runs used 0.1 % TFA (trifluoroacetic acid) in water (solvent A) and 90 % acetonitrile in water with 0.1% TFA (solvent B). For all runs, a 20-minute linear gradient with

increasing buffer B concentration was applied. Electrospray ionization mass spectrometric analysis (ESI-MS) was performed on a Bruker Daltonics MicrOTOF-Q II mass spectrometer. Fluorescent anisotropy was measured using a fluorolog®-3 Model FL3-11 fluorimeter (Horiba Jobin Yvon). Coomassie stained gels and dot blots were imaged on a LI-COR Odyssey Infrared Imager. In-gel fluorescence, chemoluminescence and autoradiogram were visualized using the GE ImageQuant LAS 4000. Scintillation counting was carried out on a Perkin Elmer 2450 microplate counter. Concentration of DNA, peptide and protein samples was measured on nanodrop2000 spectrometer from Thermo scientific or UV-vis 8453 from Agilent.

Molecular cloning strategies

Amino acid sequences of full-length AgrC-I (1-430) and AgrA (1-238) were obtained from the NCBI protein database (Refseq accession: YP_001332979.1 and YP_001332980.1). The cDNA sequences were back-translated from the amino acid sequences with optimized codons according to the default *E. coli* codon usage table (Grote et al., 2005). The cDNA were synthesized by Genewiz and received in pUC57 vectors. Coding sequences corresponding to full-length AgrC-I or AgrC-I$^{\mathbf{205\text{-}430}}$ were amplified with KOD polymerase using primers harboring appropriate restriction sites and cloned between NdeI and XhoI sites of a pET24b or a pET15b vector, respectively. Similarly, the coding sequence of full-length AgrA was cloned into a pACYCDuet vector between BamHI and XhoI restriction sites. Site-directed mutagenesis of the AgrC-I construct was performed using a QuikChange Site-Directed Mutagenesis kit using standard protocols.

In all GCN4-AgrC-I chimeras, the N-terminal portion corresponds to residues 250-274 of the Gcn4p protein in *Saccharomyces cerevisiae* (Refseq accession: NP_010907), which we refer to as GCN4$^{\mathbf{1\text{-}25}}$. The coding sequence of GCN4$^{\mathbf{1\text{-}25}}$ was fused immediately upstream of the appropriate AgrC-I fragment (residues [205-219]-430) and inserted into a pET15b vector as follows. First, the coding sequence of GCN4$^{\mathbf{1\text{-}25}}$ was amplified from synthetic cDNA with an upstream overhang overlapping with the vector sequence encoding the thrombin recognition site. Then, for each construct, the AgrC-I portion was amplified with two overhangs: the upstream one overlapped with coding sequence of GCN4$^{\mathbf{20\text{-}25}}$, while the downstream one overlapped with the vector sequence between the XhoI site and the T7-terminator. Overlap extension of an

equimolar mixture of the two above fragments followed by PCR amplification yields a pair of megaprimers containing the chimera construct that overlaps with the expression vector on both ends. These megaprimers were inserted into the vector using Phusion High-Fidelity PCR kit as described (Bryksin and Matsumura, 2010).

Bioinformatic tools used for the analysis of HPK10 homologs

To reduce the redundancy of hit sequence obtained from the PHI-BLAST, the CD-HIT program was used to cluster near-identical sequences with an identity threshold of 80% (Huang et al., 2010). One representative sequence from each cluster was included in the non-redundant sequence collection. The non-redundant sequences were aligned using COBALT for the detection of the CA domain (Papadopoulos and Agarwala, 2007). False (non-RHK) hits with a lack of 'G2-box' were removed (Dutta and Inouye, 2000).

TMH prediction was performed using the TMHMM-2.0 software package with default settings (Krogh et al., 2001). The MUSCLE program was used to generate sequence alignment for the 286 sequences predicted to possess five or more TMHs, from which the sub-alignment shown in Figure 1C was derived (Edgar, 2004). A HMM was built from the alignment. Representative sequences of each taxonomic family were aligned to the HMM, using HMMER-3.0 protocol (Eddy, 1998). For the 'G1-box' alignment shown in Figure 1B, the sequence of EnvZ (Refseq accession: NP_417863.1) was aligned, along with HPK10 subfamily sequences, to the HMM of the GHKL superfamily (PF02518) (Finn et al., 2006).

Expression and purification of recombinant proteins

With an exception of AgrA, all soluble proteins in this study were prepared in the following manner: *E. coli* BL21(DE3) cells transformed with the appropriate expression plasmid were grown at 37 °C in one liter of LB medium containing selection antibiotics at appropriate concentrations (100 μg/mL ampicillin, 50 μg/mL kanamycin or 35 μg/mL chloramphenicol). When the OD_{600} reached 0.6, the medium was cooled down to 22°C and overnight expression was induced by addition of 0.5 mM IPTG. Cells were harvested at 6000g for 20 min and the cell pellets were resuspended in 20 mL of lysis buffer (20 mM Tris, 100 mM NaCl, 1mM TECP and 1mM PMSF, pH 8.0). Cells were lysed by four passages through a French-press homogenizer.

After centrifugation at 30000g for 30min, supernatant from the cell lysate was mixed with 4 mL of Ni-NTA resin. After incubation at 4 °C for 60 minutes, the resin was repacked in a 25-mL Bio-Rad disposable plastic column. The flow-through was discarded and the column was washed with 5 column volumes (CV) of wash buffer 1 (20 mM Tris, 500 mM NaCl, 1mM TECP and 15 mM imidazole, pH 8.0) and 10 CV of wash buffer 2 (20 mM Tris, 100 mM NaCl, 1mM TECP and 25 mM imidazole, pH 8.0). Bound protein was eluted with 1.5CV of elution buffer (wash buffer 2 with 300 mM imidazole). The elution containing up to 10 mg protein was concentrated to 1mL and further purified on Superdex200 size-exclusion chromatography, from which the desired peak fractions were collected. All GCN4-AgrC-I chimera proteins were treated with thrombin for His_6-tag removal prior to the size-exclusion chromatography step. For purification of AgrA, modification to the above protocol involved a lowered expression temperature (at 16 °C) and inclusion of glycerol at 20% (v/v) in all buffers.

For membrane-bound AgrC-I constructs, *E. coli* C43(DE3) cells transformed with the appropriate expression plasmids were grown in LB broth to an OD_{600} of 1.0 and then induced at 22^{o}C with 0.5 mM IPTG overnight expression. Cells collected from one liter of culture were resuspended in 18 mL lysis buffer and disrupted in four passages through a French-press homogenizer. Cell-wall debris was spun down at 15000G for 10 min and removed. Cell-membrane vesicles were then pelleted by ultracentrifugation at 200,000g for 1 h. The membrane fraction was extracted using 5mL of buffer containing 20 mM Tris-HCl pH 8.0, 100 mM NaCl, 2% (w/v) Fos-choline-12 for 3 h at 4 °C. After another ultracentrifugation step at 100,000g for 20 min, the supernatant was subjected to Ni-NTA affinity chromatography as described above for soluble proteins, and the elution containing the target protein were further purified over a Superdex200 size-exclusion column. 0.05% (w/v) Fos-choline-14 was included in all buffers used in these chromatographic steps.

Membrane scaffold protein (MSP) and lipid stocks for nanodisc assembly

The membrane scaffold protein, MSP1E3D1, was prepared as reported (Ritchie et al., 2009). The His_7-tag on the recombinant protein was removed through TEV-protease digestion followed by anion exchange chromatography with a Hiprep Q FF 16/10 column (GE Healthcare). DMPC (1,2-*di*myristoyl-sn-glycero-3-*p*hosphocholine), DMPG (1,2-*di*myrsitoyl-sn-glycero-3-*p*hospho-

(1'-rac-glycerol)), POPE (1-palmitoyl-2-oleoyl-sn-glycero-3-phosphoethanolamine) and DMPS (1,2-dimyristoyl-sn-glycero-3-phospho-L-serine) were dried from organic solvents as described on the Avanti Polar Lipids website and prepared in 50mM-stocks solubilized in a buffer containing 20 mM Tris pH = 8.0, 100 mM NaCl, 5 mM TCEP and 150 mM sodium cholate.

Co-migration assays employing FAM-AIP-I

AgrC-I discs or empty discs (1.5 nmol) were incubated with 10 nmol FAM-AIP-I in 500 μL of nanodisc buffer at 30^{o}C for 30min. The mixture was then resolved on Superose6 size-exclusion chromatography running with nanodisc buffer. The eluate was collected in 0.25-mL size fractions, and fluorescence intensity (λ_{ex} = 490 nm, λ_{em} = 520nm) of the fractions was recorded on a Molecular Devices Spectramax M3 micro plate reader. The fluorescence intensity was plotted with the elution volume of the fraction and connected with a smoothed line. This fluorescence chromatogram overlaid with the UV chromatogram recorded by the UV detector (λ= 280 nm) is shown in Figure S3D.

AIP Stability Assays

AIP-I or AIP-II (2 nmol) was incubated in 100 μL solution buffered at pH = 7.0 for 3hrs (AIP-I) or at pH = 8.0 for 1hr (AIP-II) at 37^{o}C in the presence or absence of 0.2 nmol of AgrC-I discs. Control samples without incubation were also prepared. To each sample was added 50 μL of acetonitrile, and the mixture was centrifuged at 17000G for 5 minutes. Supernatant was analyzed by RP-HPLC on a C18 column using a 0-70B% gradient. The percentage of intact AIPs remaining after incubation with buffer or AgrC-I discs was determined from the peak area and plotted as mean ± SD (n=3) in Figure S4A.

Detection of phosphorylated AgrC-I or AgrC-I variants: general considerations

In this work, we employed a few different readouts to detect and quantify the phosphorylation levels of AgrC-I or AgrC-I variants. Anti-pHis dot blot was the method of choice due to the high throughput of analysis (Kee et al., 2013). Therefore, most kinetic studies for the forward and reverse autophosphorylation of AgrC-I were performed based on dot-blot assays. We also employed anti-pHis western blotting in fixed time-point assays to identify the phosphorylated species based on band positions. For some experiments we employed a more classic

radiolabeling assay using [γ-^{32}P]-ATP as the phosphoryl donor and employing autoradiograghy as the readout. This was found to be especially useful when comparing the activity of different AgrC-I constructs and GCN4-AgrC-I chimeras due to concerns that immunodetection assays might be unduly influenced by subtle differences in the transfer or detection properties of each construct.

Autophosphorylation of AgrC-I

All autokinase reactions were performed in reaction buffer containing 50 mM Tris-HCl, 15 mM HEPES-Na pH = 7.8, 100 mM NaCl, 5 mM $MgCl_2$ and 1 mM TCEP. AIPs were included as indicated (from DMSO stocks), and DMSO was added to make the overall DMSO concentration up to 1% (v/v). Typically, an autokinase reaction contained 20 μM [γ-^{32}P]-ATP (1Ci/mmol) or 1 mM regular ATP or GTP and 1.4 μM dimeric receptor (full-length AgrC-I variants embedded in nanodiscs, or GCN4-AgrC-I chimeras) unless otherwise indicated. The reaction was incubated at 37 °C. In fixed time point assays, reactions were performed for 40min with [γ-^{32}P]-ATP or 3min with regular nucleotides. For time courses, samples were withdrawn from the reaction at indicated time points and quenched with gel loading buffer. All samples were processed, according to the specified method of detection, as described in the following sections.

Phospho-relay from AgrC-I to AgrA

AgrC-I discs were phosphorylated in the absence of AIP with 50 μM [γ-^{32}P]-ATP at 37^{o}C for 90 min, and subsequently exchanged into an ATP-free reaction buffer (50 mM Tris-HCl, 15 mM HEPES-Na pH = 7.8, 100 mM NaCl and 1 mM TCEP) using Bio-Rad Micro Bio-Spin™ P-6 Gel Columns. This step gave rise to a stock containing 1.2 μM of AgrC-I disc with 0.25 μM of pHis as quantified through scintillation counting. The stock was equally divided into three portions, to which was added either AIP stocks or DMSO at equal volume. These pre-phosphorylated AgrC-I samples were mixed 1:1 with AgrA protein (3.6 μM stock in 50 mM Tris-HCl pH 8.0, 100 mM NaCl , 5 mM TCEP in 20% (v/v) glycerol) to initiate the phospho-relay. The AgrA buffer was used to mix with AgrC-I samples in mock reactions. All reactions were incubated at 37^{o}C from which samples were withdrawn at indicated time points and quantified through autoradiography.

Phospho-relay from GC214 to AgrA and AgrA dephosphorylation

GC214 (10 μM dimer) was treated with 100 μM [γ-^{32}P]-ATP in 20-μL volume at 37^{o}C for 90 min, and subsequently exchanged into an ATP-free reaction buffer. The product was diluted to 180 μL for a stock containing 0.40 μM GC214 dimer (RP-HPLC) with 0.73 μM of pHis (scintillation counting). To initiate the reaction, a mixture containing AgrA, AgrC-I discs and/or AIP peptide were pre-incubated at 37^{o}C for 2min, to which ^{32}P-labeled GC214 was then added. Final concentration of each component (if present) was 0.1 μM for GC214 dimer, 2.0 μM for AgrA, 2.0 μM for AgrC-I discs and 10 μM for AIP-I or AIP-II. All reactions were incubated at 37^{o}C from which samples were removed at indicated time points and quantified through autoradiography.

Reverse Autophosphorylation of AgrC-I

AgrC-I discs were phosphorylated in the absence of AIP with 2.0 mM of regular ATP at 37^{o}C for 60min and subsequently exchanged into an ATP-free reaction buffer (50 mM Tris-HCl, 15 mM HEPES-Na pH = 7.8, 100 mM NaCl and 1 mM TCEP) using a Superose6 size-exclusion column (Figure S4G). This step gave rise to a stock containing 4.0 μM of AgrC-I disc and 4.2 μM of pHis as quantified relative to an intermediate standard standardized with scintillation counting. The pHis level of this stock was stable at 4^{o}C over 2 months (data not shown). The stock was diluted 4 fold in reaction buffer in the presence of varying levels of ADP (0-2 mM), $MgCl_2$ (5mM) and either AIP-I (10 μM from a DMSO stock) or DMSO (1% v/v). The reaction was incubated at 37^{o}C from which samples were withdrawn at indicated time points and analyzed using anti-pHis dot blot.

Scintillation counting

Samples from each reaction were spotted on nitrocellulose membranes in triplicate. Samples from a mock reaction (in the absence of AgrC-I) under the same conditions were also spotted and used as the background. Each spot was 5 μL in volume. The membranes were air-dried and then washed 3x5min with TBST buffer (50mM Tris pH 8.5, 150 mM NaCl and 0.1% (v/v) Tween-20) and air-dried again. Each piece of membrane was subsequently transferred to a 4mL counting vial containing 3.5mL of Ultima Gold™ Cocktails (Perkin Elmer) and luminescence from the vial was quantified in a scintillation counter. For quantification purposes, an aliquot of the [γ-

^{32}P]-ATP stock used in the reactions was diluted into a series of samples of known concentration. These samples were spotted (5 μL) in duplicate on nitrocellulose membranes and counted after drying without TBST-wash. Correlations between count numbers (in *c*ount *p*er *m*inute, CPM) and concentrations of [γ-^{32}P]-ATP dilutions were plotted to give a working curve which was used to calculate the absolute pHis concentration in the background corrected experimental samples.

Autoradiography

For detection using autoradiography, samples from autokinase or phospho-relay reactions were mixed with 4x SDS sample buffer (1x concentration: 50 mM Tris-HCl pH 8.0, 2 % (w/v) SDS, 10 (v/v) % glycerol, 10 mM dithiothreitol and 0.01 (w/v) % bromophenol blue) and immediately resolved on a 15% Tris-HCl SDS-polyacrylamide gel. The gel was then dried, and incubated with Eastman Kodak BIOMAX MR film for 5 hrs at RT. After development, the autoradiogram (film) was scanned using ImageQuant LAS 4000 (GE).

For quantification purposes, a highly phosphorylated AgrC-I stock was diluted into a series of internal standards. pHis concentrations of these standards were assigned in arbitrary units based on the dilution process. These standards were resolved on a denaturing gel and exposed, along with gels bearing all experimental samples, to the same piece of film. Importantly, loading volumes of all experimental and standard samples was identical. The normalized, background-subtracted intensity of all bands on the autoradiogram was calculated using the ImageQuant TL program, and used to generate a working curve from which pHis levels (arbitrary units) of experimental samples were determined.

Anti-pHis western blot

As in autoradiography, samples from autokinase reactions were mixed with 4x SDS sample buffer and resolved on a 15% Tris-HCl SDS-polyacrylamide gel. Then, anti-pHis western blot was performed as reported (Kee et al., 2013). Briefly, the resolved proteins were electroblotted onto a PVDF membrane at 100 V for 1hr. The membrane was blocked with 3% BSA in TBST for 30min and incubated with anti-pHis antibody diluted 1:500 in TBST with 3% BSA for 1 hr at RT. After washing with TBST (3 x 5 min), the membrane was then incubated with goat anti-

rabbit IgG-HRP conjugate (diluted 1:5000 in wash buffer with 3% BSA) for 1 hr at RT, followed by washing with TBST (3 x 5 min). The membrane was incubated with ECL chemiluminescence solution for 1 min at RT and chemiluminescence from the membrane was imaged using ImageQuant LAS 4000. The membrane was washed with water and stained with Coomassie blue for the visualization of loading control.

Anti-pHis dot blot

Nitrocellulose membrane (8cm x 8cm) was gridded 10 x 10 and heated on a 50^{o}C heat block prior to use. 2-μL samples from forward or reverse autokinase reactions were directly spotted at the center of each small square. Internal standards of known absolute or normalized pHis levels were also spotted (2 μL) in duplicate on the same membrane. The membrane was allowed to dry, cooled to RT and blocked with 3% BSA in TBST for 30min. Anti-pHis antibody diluted 1:500 in TBST with 3% BSA was added for 1 hr at RT. After washing with TBST (3 x 5 min) the membrane was incubated with IRDye 800CW goat anti-rabbit IgG (diluted 1:15000 in wash buffer with 3% BSA) for 1 hr at RT, followed by washing with TBST (3 x 5 min). The dot blot was imaged on a LI-COR Odyssey Infrared Imager and the intensity of each dot was calculated using the built-in densitometry software. The dot blot was washed with water and stained with Coomassie blue for the visualization and quantification of loading. The pHis concentration of each sample was determined using a working curve generated from the intensity-to-concentration relationship of standard samples.

Data processing for kinetic parameters

For kinetic studies, time course experiment of a reaction was performed in multiplicate (n = 3 or 4). The time courses were averaged and fit to certain kinetic models, returning kinetic parameters of the subject reaction. Curve fitting were performed using Graphpad Prism Software.

A. Phospho-relay from AgrC-I to AgrA (quantified using autoradiography)

AgrC-I~P + AgrA → AgrA~P + AgrC-I

AgrA~P + H_2O → AgrA + Pi (Scheme 1)

where, AgrC-I~P and AgrA~P represent phosphorylated AgrC-I and AgrA, respectively. To study the decay of AgrC-I~P, only the kinetic equation of the first reaction is considered:

$$\frac{d[\text{AgrC–I}\sim\text{P}]}{dt} = -k[\text{AgrC–I}\sim\text{P}][\text{AgrA}] \qquad \text{(eq. 1)}$$

where [AgrC-I~P] is the concentration of AgrC-I~P monomers, [AgrA] is the concentration of AgrA, k is the second-order kinetic constant and t is time. In the experimental setup, [AgrC-I~P] << [AgrA] at t =0. Therefore, progress of the reaction has negligible affect on [AgrA] such that the phospho-relay follows near-first-order kinetics with respect to AgrC-I~P. Hence, [AgrC-I~P] (in arbitrary unit) was normalized to the [AgrC-I~P] at t = 0, and the time course was fit to the eq. 2:

$$\frac{[\text{AgrC–I}\sim\text{P}]}{[\text{AgrC–I}\sim\text{P}]\big|^{t=0}} = (1 - plateau)\bullet\exp(-k_{app}\bullet t) + plateau \qquad \text{(eq. 2)}$$

where k_{app} is the apparent first-order kinetic constant and *plateau* represents the un-reactable fraction of AgrC-I~P at $t = 0$. The apparent half-life of AgrC-I~P, $t_{1/2}$, was obtained from eq. 3:

$$t_{1/2} = \frac{\ln 2}{k_{app}} \qquad \text{(eq. 3)}$$

B. Phospho-relay from GC214 to AgrA and self-catalyzed dephosphorylation of AgrA (quantified using autoradiography)

GC214~P + AgrA → GC214 + AgrA~P

AgrA~P + H_2O → AgrA + Pi (Scheme 2)

where, GC214~P and Pi represents phosphorylated GC214 and inorganic phosphate, respectively. This reaction scheme is similar to Scheme 2 but quantitatively different because the unmodified GC214 is present in much smaller amount. This drives the phospho-transfer reaction to near completion in approximately one minute (Figure 3H and S3F). Thereafter, no change in [GC214~P] is observed and therefore the change in [AgrA~P] accounts only to the self-catalyzed dephosphorylation (the second reaction). Therefore, [AgrA~P] values (in arbitrary unit) after t = 1min were fit to the first-order decay model for the kinetic constant. The apparent half-life of AgrA-I~P was also calculated using eq. 3.

C. Autokinase reaction of AgrC-I (quantified using autoradiography)

AgrC-I + ATP → AgrC-I~P + ADP (Scheme 3)

The initial velocity of the reaction follows eq. 4:

$$v_i = \left.\frac{\mathrm{d}[\mathrm{AgrC{-}I{\sim}P}]}{\mathrm{d}t}\right|^{t=0} = k_1[\mathrm{AgrC{-}I}] \qquad \text{(eq. 4)}$$

where [AgrC-I~P] is the concentration of AgrC-I~P monomers, [AgrC-I] is the concentration of free AgrC-I monomers, v_i is the initial velocity and k_1 is the apparent rate constant. The concentration of AgrC-I discs was 1.4 μM (2.8 μM of each monomer) and [γ-^{32}P]-ATP was used at 20 μM. Thus, v_i should be proportional to k_1. In all reactions, [AgrC-I~P] (in arbitrary unit) increased linearly over the first 40 minutes; $R^2 > 0.90$. Therefore, v_i was calculated as the slope of the [AgrC-I~P] time course. For ease of comparision, v_i found under different conditions was normalized to the v_i in the absence of AIP and plotted versus the equivalence of AIP-I (Figure 4A).

C. Autokinase reaction of AgrC-I (quantified using anti-pHis dot blot)

Taking the influence of substrate concentration, [ATP] into account, the initial velocity of the reaction is given in eq. 5:

$$v_i = \left.\frac{\mathrm{d}[\mathrm{AgrC{-}I{\sim}P}]}{\mathrm{d}t}\right|^{t=0} = k_1[\mathrm{AgrC{-}I}] = k_{\max}\frac{[\mathrm{ATP}]}{K_m + [\mathrm{ATP}]}[\mathrm{AgrC{-}I}] \qquad \text{(eq. 5)}$$

where k_1 is the first-order rate constant at a given ATP concentration, k_{max} is the first-order rate constant assuming that ATP saturates the binding sites on AgrC-I and K_m is the apparent Michaelis constant with respect to ATP. Under the conditions employed, consumption of ATP was negligible. Therefore, the reaction was first-order with respect to AgrC-I. Determination of K_m and k_{max} entails k_1 values at a series of ATP concentrations to be calculated from v_i and [AgrC-I]. v_i values were either obtained from linear regression as described in section B or, in the case of saturable time courses, using eq. 6:

$$[\mathrm{AgrC{-}I{\sim}P}] = plateau \bullet \left(1 - \exp\left(-k \bullet (t - t_0)\right)\right) \qquad \text{(eq. 6)}$$

where *plateau* is the saturation level of pHis, and t_0 is a lag time used to offset the systematic error on the reaction time elapsed before sampling the first time point.

The apparent rate constant k_1 was calculated using eq. 7:

$$k_1 = \frac{plateau \bullet k}{[\mathrm{AgrC{-}I}]\big|^{t=0}} \qquad \text{(eq. 7)}$$

The k_1-[ATP] relationship of AgrC-I discs in different ligand states was fit to the Michaelis-Menten equation (eq. 8), returning k_{max} and K_m values as fitting parameters:

$$k_1 = k_{\max} \frac{[\mathrm{ATP}]}{K_m + [\mathrm{ATP}]} \qquad \text{(eq. 8)}$$

D. Reverse autokinase reaction (quantified using anti-pHis dot blot)

AgrC-I~P + ADP → AgrC-I + ATP (Scheme 4)

Taking the influence of substrate concentration, [ADP], into account, the initial velocity of the reaction is given in eq. 9:

$$v_i = -\left(\frac{\mathrm{d}[\mathrm{AgrC{-}I{\sim}P}]\big|^{t=0}}{\mathrm{d}t}\right) = k_{-1}[\mathrm{AgrC{-}I{\sim}P}] = k_{\max}\frac{[\mathrm{ADP}]}{K_m + [\mathrm{ADP}]}[\mathrm{AgrC{-}I{\sim}P}] \qquad \text{(eq. 9)}$$

where k_{-1} is the first-order rate constant at a given ADP concentration, k_{max} is the first-order rate constant assuming that ADP saturates the binding sites on AgrC-I and K_m is the apparent Michaelis constant with respect to ATP. In contrast to the forward reaction, the reverse reaction is first-order with respect to [AgrC-I~P] at any practical ADP concentration. Absolute quantification of [AgrC-I~P] is hence not required. Therefore, the starting material, pre-phosphorylated AgrC-I discs, was used for internal standardization, and [AgrC-I~P] at all time points was quantified relative to the starting point. As all time courses saturated at the end of the assays, they were fit to eq. 10:

$$[\mathrm{AgrC{-}I{\sim}P}] = (Y0 - plateau) \bullet \exp(k_{-1} \bullet t) + plateau \qquad \text{(eq. 10)}$$

The k_1-[ADP] relationship of AgrC-I discs in different ligand states was fit to the Michaelis-Menten equation (eq. 11), returning k_{max} and K_m values as fitting parameters:

$$k_{-1} = k_{\max} \frac{[\mathrm{ADP}]}{K_m + [\mathrm{ADP}]} \qquad \text{(eq. 11)}$$

Fluorescent anisotropy measurements

Fluorescence measurements were performed in measurement buffer (20 mM HEPES, pH 7.0, 100 mM NaCl, 1mM TCEP, 2 μM BSA and 100 nM of empty nanodiscs). All buffers were freshly degassed before use. Measurement of fluorescent anisotropy was performed on a Fluorolog-3 instrument (HORIBA Jobin Yvon) equipped with automated dual polarizers and using a Semi-Micro Fluorometer Cell (Starna Cells) with a 10-mm path length. The measurement chamber was held at a constant temperature of 30.0°C by an Advanced Series AC200 thermostat (Thermo Scientific) connected to an Arctic series refrigerated circulating water bath (Thermo Scientific). The excitation wavelength was 490 nm and emission wavelength was recorded at 520 nM, both with a bandwidth of 5 nm. Six to eight measurements were taken per titration point with an integration time of 2 sec for V/V, V/H, H/H and H/V polarizer settings (excitation/emission, V: vertical polarization, H: horizontal polarization). The final anisotropy, *r,* was calculated from $r = (I_{VV} - G \times I_{VH})/(I_{VV} + 2 \times G \times I_{VH})$, with $G = I_{HV}/I_{HH}$.

For titrations of FAM-AIP-I with AgrC-I discs, 750 μL of measurement buffer containing 2.0 nM FAM-AIP-I was transferred to the cuvette and the fluorescent anisotropy was measured as a reference. AgrC-I discs were then added to the required concentration and the mixture allowed to equilibrate for 5 minutes before taking the anisotropy measurement. This process was repeated until measurement of the last titration point (at 1.5 μM of AgrC-I discs). Each titration of FAM-AIP-I was performed simultaneously with a control titration, in which 2.0 nM of FAM-(lin)-AIP-I was included at the starting point.

For competitive titrations with AIP-I or AIP-II, the fluorescent anisotropy of 750 μL of measurement buffer containing 20 nM FAM-AIP-I was first measured as a reference. The starting-point mixture was then prepared by addition of AgrC-I discs to a final concentration of 150nM. The desired AIP was titrated into the cuvette and the anisotropy measured after 5 minutes equilibration.

Data processing of fluorescent-anisotropy-based binding assays

Curve fitting were performed using Graphpad Prism Software.

A. Titrations of FAM-AIP-I with AgrC-I discs

The fluorescent anisotropy change, Δr, was calculated for each titration point as:

$$\Delta r = r - r_r \qquad \text{(eq. 12)}$$

where r_r is the reference anisotropy measured in the absence of AgrC-I discs. To correct the anisotropy increase due to the light-scattering effect of AgrC-I discs, observable only at high-nanomolar and above, the anisotropy change in the control titration (titration of FAM-(lin)-AIP-I), Δr_c, was subtracted from the anisotropy change in the experimental titration, Δr_o at each AgrC-I concentration. This resulting correction, $\Delta r_o - \Delta r_c$, reflects the anisotropy change caused by binding of FAM-AIP-I to the AgrC-I discs. Therefore, $\Delta r_o - \Delta r_c$ (referred to as ΔSSA^c in Figure 4B) was plotted against [AgrC-I disc]. In titrations with AgrC-I$^{S109V S116I}$ mutant discs, no significant increase of $\Delta r_o - \Delta r_c$ was observed so that data points were connected with a smoothed line. In titrations with AgrC-I WT discs, the dataset was fit to the Hill equation treating AgrC-I as the ligand (eq. 13):

$$\frac{\Delta r_0 - \Delta r_C}{\Delta r_{\max}} = \frac{[\text{AIPI}_{\text{bound}}]}{[\text{AIPI}_{\text{total}}]} = \frac{[\text{AgrC–I disc}]^h}{[\text{AgrC–I disc}]^h + K_d} \qquad \text{(eq. 13)}$$

where $[\text{AIPI}_{\text{bound}}]$ is the concentration of FAM-AIP-I bound to AgrC-I, $[\text{AIPI}_{\text{total}}]$ is the total concentration of FAM-AIP-I, K_d is the dissociation constant, h is the Hill coefficient with respect to AgrC-I, and Δr_{max} is the $\Delta r_o - \Delta r_c$ value assuming 100% binding of FAM-AIP-I to AgrC-I discs. Δr_{max}, K_d, and h were obtained as fitting parameters.

To obtain the Hill coefficient with respect to FAM-AIP-I, we considered the Hill equation treating FAM-AIP-I as ligand:

$$\frac{[\text{AgrC–I}_{\text{bound}}]}{[\text{AgrC–I}_{\text{free}}]} = \frac{[\text{AIPI}_{\text{free}}]^h}{K_d} \qquad \text{(eq. 14)}$$

where $[\text{AgrCI}_{\text{free}}]$ and $[\text{AgrC-I}_{\text{bound}}]$ are the concentration of AgrC-I sites unoccupied and bound to FAM-AIP-I, respectively, and $[\text{AIPI}_{\text{free}}]$ is the unbound FAM-AIP-I concentration.

Importantly, AIP-I was found to bind AgrC-I in 2:2 stoichiometry. For each titration point, [AgrC-I_{free}], [AgrC-I_{bound}] and [$AIPI_{free}$] could be calculated as following:

$$[\mathrm{AIPI_{free}}] = 2.0\mathrm{nM} \times \frac{750\mu\mathrm{L}}{V_{total}} \times \left(1 - \frac{\Delta r_0 - \Delta r_C}{\Delta r_{\max}}\right) \qquad \text{(eq. 15)}$$

$$[\mathrm{AgrC{-}I_{bound}}] = [\mathrm{AIPI_{bound}}] = 2.0\mathrm{nM} \times \frac{750\mu\mathrm{L}}{V_{total}} \times \frac{\Delta r_0 - \Delta r_C}{\Delta r_{\max}} \qquad \text{(eq. 16)}$$

$$[\mathrm{AgrC{-}I_{free}}] = 2 \times [\mathrm{AgrC{-}I\ disc}] - [\mathrm{AgrC{-}I_{bound}}] \qquad \text{(eq. 17)}$$

Where V_{total} is the total volume of the titration system including the volume of titrant added. $\frac{[\mathrm{AgrC\text{-}I_{bound}}]}{[\mathrm{AgrC\text{-}I_{free}}]}$ was then plotted with [$AIPI_{free}$]. To avoid large relative errors in [$AIPI_{free}$] and [AgrC-I_{bound}], only data points meeting the criterion of $0.15 < \frac{\Delta r_0 - \Delta r_C}{\Delta r_{\max}} < 0.85$ were included in the dataset. Fitting the dataset to the eq.14 returned values of K_d and h. K_d and h from four individual titrations were pooled and shown as mean ± SD in the main text.

B. Competitive titrations with native AIPs

The fluorescent anisotropy change, Δr (referred to as ΔSSA in Figure 4C), was calculated for each titration point and plotted with the concentration of [AIP] in a semi-log plot. Since FAM-AIP-I was found to bind AgrC-I non-cooperatively, we treated AgrC-I as independent monomers. The dataset was fit to eq. 18, which was simplified from the literature (Swillens, 1995):

$$\Delta r = \frac{(S + B_{\max}) - \sqrt{(S + B_{\max})^2 + 4 \times \Delta r_{\max} \times B_{\max}}}{2}, \text{ where } \quad S = \left(\frac{K_{d,\mathrm{AIP}} + [\mathrm{AIP}]}{K_{d,\mathrm{AIP}}} \bullet \frac{K_{d,\mathrm{FAM-AIPI}}}{20\mathrm{nM}} + 1\right) \bullet \Delta r_{\max} \qquad \text{(eq. 18)}$$

In the above, $K_{\mathbf{d,\ FAM\text{-}AIP}}$, the dissociation constant of FAM-AIP-I, was 122nM. $\Delta r_{\mathbf{max}}$, the anisotropy change assuming 100% binding of FAM-AIP-I to AgrC-I disc, was calculated from the Δr and the concentration of FAM-AIP-I and AgrC-I disc at the starting point. $B_{\mathbf{max}}$ was calculated as:

$$B_{\max} = \Delta r_{\max} \bullet \frac{[\mathrm{AgrC{-}I_{total}}]}{[\mathrm{FAM{-}AIPI_{total}}]} \qquad \text{(eq. 19)}$$

$K_{d,\,\mathbf{AIP}}$, the dissociation constant of native AIP, was the only variable parameter in the fitting process. For each AIP, K_d values obtained from three individual titrations were pooled and shown as mean ± SD in the main text.

Solid-phase peptide synthesis

Wild-type and mutant linker peptides were synthesized using Fmoc-based solid phase peptide chemistry on a Rink-amide MBHA resin (0.59 mmol/g). Synthesis was carried on a Liberty Synthesizer. Chain assembly was carried out with HATU (4.9 eq.) activation using a 5-fold excess of standard N^{α}-Fmoc protected amino acid over the resin in DMF with DIEA (8 eq.). The Fmoc protecting group was removed with 20% piperidine in DMF. Peptides were cleaved from the resin with a cocktail containing 95% TFA (v/v), 2.5% TIS (v/v) and 2.5% water (v/v). Crude peptide products were precipitated and washed with cold ether, dissolved in HPLC solvent A and then purified by RP-HPLC.

Circular-dichroism (CD) analysis of the TMH-DHp linker peptides

CD spectra were taken on a Chirascan^{TM} CD spectrometer equipped with a Quantum TC125 temperature control unit at 20^{o}C. Path length of the cuvette was 1mm. The HPLC-purified peptide was dissolved in a 100-μM stock solution. This stock was diluted into 15-μM samples containing 10 mM sodium phosphate pH = 7.0, 50 mM NaF, and 0%, 10%, 20%, 30%, 40% or 50% TFE (v/v). For each peptide, CD spectra of six samples were corrected for buffer background and Helical content (H) was calculated as:

$$H = \frac{\theta_{222}}{\theta_{\max}} = \frac{\theta_{222}}{-40000 \bullet (1 - 2.5/n) + 100 \bullet T} \qquad \text{(eq. 20)}$$

where θ_{222} is the mean residue ellipticity at 222 nm in (deg·cm^2·dmol^{-1}), n is the length of the peptide (in residue) and T is temperature in ^{o}C (Scholtz et al., 1991).

Supplemental References

Bryksin, A.V., and Matsumura, I. (2010). Overlap extension PCR cloning: a simple and reliable way to create recombinant plasmids. Biotechniques *48*, 463-465.

Davis, J.J., Xia, F., Overbeek, R.A., and Olsen, G.J. (2013). Genomes of the class Erysipelotrichia clarify the firmicute origin of the class Mollicutes. International journal of systematic and evolutionary microbiology *63*, 2727-2741.

Dutta, R., and Inouye, M. (2000). GHKL, an emergent ATPase/kinase superfamily. Trends Biochem Sci *25*, 24-28.

Eddy, S.R. (1998). Profile hidden Markov models. Bioinformatics *14*, 755-763.

Edgar, R.C. (2004). MUSCLE: multiple sequence alignment with high accuracy and high throughput. Nucleic Acids Res *32*, 1792-1797.

Finn, R.D., Mistry, J., Schuster-Bockler, B., Griffiths-Jones, S., Hollich, V., Lassmann, T., Moxon, S., Marshall, M., Khanna, A., Durbin, R*., et al.* (2006). Pfam: clans, web tools and services. Nucleic Acids Res *34*, D247-D251.

Grote, A., Hiller, K., Scheer, M., Munch, R., Nortemann, B., Hempel, D.C., and Jahn, D. (2005). JCat: a novel tool to adapt codon usage of a target gene to its potential expression host. Nucleic Acids Res *33*, W526-W531.

Huang, Y., Niu, B.F., Gao, Y., Fu, L.M., and Li, W.Z. (2010). CD-HIT Suite: a web server for clustering and comparing biological sequences. Bioinformatics *26*, 680-682.

Krogh, A., Larsson, B., von Heijne, G., and Sonnhammer, E.L.L. (2001). Predicting transmembrane protein topology with a hidden Markov model: Application to complete genomes. J Mol Biol *305*, 567-580.

Papadopoulos, J.S., and Agarwala, R. (2007). COBALT: constraint-based alignment tool for multiple protein sequences. Bioinformatics *23*, 1073-1079.

Scholtz, J.M., Qian, H., York, E.J., Stewart, J.M., and Baldwin, R.L. (1991). Parameters of Helix-Coil Transition Theory for Alanine-Based Peptides of Varying Chain Lengths in Water. Biopolymers *31*, 1463-1470.

Swillens, S. (1995). Interpretation of Binding Curves Obtained with High Receptor Concentrations - Practical Aid for Computer-Analysis. Mol Pharmacol *47*, 1197-1203.